TECHNICAL MEMORANDUMS

NATIONAL ADVISORY COMMITTEE FOR AERONAUTICS

No. 696

THE PROBLEM OF THE PROPELLER IN YAW WITH SPECIAL REFERENCE TO AIRPLANE STABILITY

By Franz Misztal

Abhandlungen aus dem Aerodynamischen Institut
an der Technischen Hochschule Aachen
No. 11, 1932

Washington
January, 1933

ant is $\frac{c'}{2}$. Then the flow attitude is defined by the velocity components w_o, $u_o = r\omega$ and u_q and the induced additive velocity $\frac{c'}{2}$. (Fig. 3.)

If the axis of rotation is parallel to the direction of flow, that is, $u_q = 0$ and $w = w_o$, the corresponding induced additive velocities would be $\frac{w'_o}{2}$, $\frac{u'_o}{2}$ and $\frac{c'_o}{2}$.

Simultaneously it is assumed in accord with the general propeller theory that the induced velocities at infinity behind the plane of the blade attain to twice the value even in the case of propeller in yaw, or in other words, that the small frictional losses on the blades and the jet contraction and autorotation of the propeller slipstream are neglected.

In agreement with the airfoil theory (fig. 3) the thrust and the tangential force of a blade element at the point (r, ϑ), relative to area $rd\vartheta dr$, are:

$$dS = [dA \cos \beta' - dW \sin \beta'] \frac{d\vartheta}{2\pi} =$$

$$\frac{c_a}{2\pi} zt\rho \frac{v^2}{2} \sin \beta' \left[\frac{1}{\tan \beta'} - \epsilon\right] dr d\vartheta \qquad (1)$$

$$dT = [dA \sin \beta' + dW \cos \beta'] \frac{d\vartheta}{2\pi} =$$

$$\frac{c_a}{2\pi} zt\rho \frac{v^2}{2} \sin \beta' \left[1 + \frac{\epsilon}{\tan \beta'}\right] dr d\vartheta \qquad (2)$$

where zt = total blade width at radius r; v = effective air flow velocity, β' = induced pitch angle, c_a = lift coefficient and ϵ = lift-drag ratio (for infinite span) of the element.

According to Figure 3:

$$\sin \beta' = \frac{w_o + \frac{w'}{2}}{v}$$

and

$$\tan \beta' = \frac{w_o + \frac{w'}{2}}{u_o + u_q - \frac{u'}{2}} = \frac{1}{\frac{u_o - \frac{u'}{2}}{w_o + \frac{w'}{2}} + u_q \frac{1}{w_o + \frac{w'}{2}}}$$

Putting:

$$\left.\begin{aligned}\eta'_\alpha &= \frac{w_o}{w_o + \frac{w'}{2}} \\ \eta'_i &= \frac{u_o - \frac{u'}{2}}{w_o + \frac{w'}{2}} \frac{w_o}{u_o}\end{aligned}\right\} \quad (3)$$

and

$$u_q = w_o \tan \varphi \sin \vartheta = w_o k, \quad (4)$$

yields

$$\sin \beta' = \frac{1}{\eta'_\alpha} \frac{w_o}{c} \quad (5)$$

$$\tan \beta' = \frac{\lambda}{\eta'_i x + \eta'_\alpha \lambda k} \quad (6)$$

wherein $x = \frac{r}{R}$ (R = outside radius) and $\lambda = \frac{w_o}{R\omega}$ = coefficient of propeller advance referred to the axial inflow velocity and v is approximately replaced by the undisturbed relative velocity c (assuming $\frac{c'}{2}$ small with respect to c (fig. 3); η'_α and η'_i correspond to the theoretical and the total induced efficiency* of the blade element in the propeller theory.

The additive tangential velocity u_q changes the effective angle of air flow of the element i by the amount Δi. Accordingly its lift coefficient is

$$c_a = c_{a_o} + \Delta i \frac{dc_a}{di}$$

Expressing

$$\frac{\frac{dc_a}{di}}{c_{a_o}} = \frac{c'_a}{c_{a_o}} = p \quad (i \text{ in radians})$$

* The formulas and concepts used, and presumed as known, are from Bienen and v. Karman's report: On the Theory of Propellers, V.D.I., 1924, p. 1237.

gives

$$c_a = c_{a_o} [1 + p \Delta i] \tag{7}$$

Making due allowance for the last relations in equations (1) and (2) we have, with $\rho \frac{w_o^2}{2} = q_o$:

$$dS = \frac{c_{a_o}}{2\pi\eta'_\alpha} (1 + p \Delta i) Rq_o zt \frac{c}{w_o}\left[\frac{\eta'_i}{\lambda} x + \eta'_\alpha k - \epsilon\right] dx d\vartheta, \tag{1'}$$

$$dT = \frac{c_{a_o}}{2\pi\eta'_\alpha} (1 + p \Delta i) Rq_o zt \frac{c}{w_o}\left[1 + \epsilon\left(\frac{\eta'_i}{\lambda} x + \eta'_\alpha k\right)\right] dx d\vartheta \tag{2'}$$

which leaves the change in angle of air flow Δi relative to φ, relative to the position of the blade element in the plane of the propeller and relative to the characteristic of the blade profile. According to Figure 3:

$$\Delta i = (\beta'_o - \beta_o) + (\beta_o - \beta) - (\beta' - \beta) \tag{8}$$

or, when replacing the small angle differences by sine values:

$$\Delta i = \frac{c'_o}{2} \frac{}{c_o} + \frac{u_q \frac{w_o}{c}}{c_o} - \frac{c'}{2c} \tag{8'}$$

The induced velocity c' can be defined by the momentum theory, whereby the small frictional losses, the jet contraction and the autorotation of the vortex system are disregarded. The velocity in point (r, ϑ) is visualized as symmetrically distributed on the periphery and we write:

$$dA = c_{a_o} (1 + p \Delta i) ztdr\rho \frac{v^2}{2} = \rho 2\pi r dr (w_o + \frac{w'}{2}) c'$$

and for the case of the propeller in axial flow of velocity w_o with equal angular velocity ω:

$$dA_o = c_{a_o} ztdr\rho \frac{v_o^2}{2} = \rho 2\pi r dr \left(w_o + \frac{w'_o}{2}\right) c'_o$$

Again v and v_o are replaced by c and c_o, so that these two equations finally become

$$\frac{c'}{c'_o} = (1 + p\Delta i)\frac{c^2}{c^2_o} \cdot b, \qquad (9)$$

where

$$b = \frac{w_o + \frac{w'_o}{2}}{w_o + \frac{w'}{2}}$$

Then, equations (8) and (9) yield:

$$\Delta i = \frac{\frac{u_q w_o}{c\, c_o} - \frac{c'_o}{2\, c_o}\left(\frac{c}{c_o} b - 1\right)}{1 + p\,\frac{c'_o}{2\, c_o}\,\frac{c}{c_o}\, b}$$

According to Figure 3:

$$c_o = \sqrt{w^2_o + u^2_\varphi} = R\omega\sqrt{x^2 + \lambda^2}$$

and, by approximation:

$$\frac{c}{c_o} = 1 + \frac{u_q\,\frac{u_o}{c_o}}{c_o} = 1 + k\lambda\frac{x}{x^2 + \lambda^2},$$

$$\frac{c_o}{c} = \sim 1 - k\lambda\frac{x}{x^2 + \lambda^2},$$

which is equivalent to neglecting the terms with k^2, and $k = \tan\varphi \sin\vartheta < 1$, or better $\tan\varphi < 1$. In addition:

$$\frac{c'_o}{2\, c_o} = \tan(\beta'_o - \beta_o) = \frac{\frac{w_o + \frac{w'_o}{2}}{u_o - \frac{u'_o}{2}} - \frac{w_o}{u_o}}{1 + \frac{w_o + \frac{w'_o}{2}}{u_o - \frac{u'_o}{2}}\,\frac{w_o}{u_o}}$$

or with

$$\frac{u_o - \frac{u'_o}{2}}{w_o + \frac{w'_o}{2}} \frac{w_o}{u_o} = \eta_i$$

$$\frac{c'_o}{2 c_o} = (1 - \eta_i) \lambda \frac{x}{\eta_i x^2 + \lambda^2} \qquad (11)$$

here η_i = induced efficiency of the blade element at radius r of propeller in axial air flow of w_o velocity.

Now equation (10) becomes:

$$\Delta i = \frac{\frac{k\lambda^2}{x^2+\lambda^2}\left(1-k\lambda\frac{x}{x^2+\lambda^2}\right) - (1-\eta_i)\lambda\frac{x}{\eta_i x^2+\lambda^2}\left[\left(1-k\lambda\frac{x}{x^2+\lambda^2}\right)b-1\right]}{1+p(1-\eta_i)\ b\left(1+k\lambda\frac{x}{x^2+\lambda^2}\right)\lambda\frac{x}{x^2+\lambda^2}} \qquad (10')$$

The determination of b is obtained from Figure 4, where $\frac{c'}{2}$ is geometrically divided into $\frac{c'_1}{2} \parallel \frac{c'_o}{2}$ and $\frac{c'_2}{2} \perp \frac{c'}{2}$ because:

$$\frac{1}{b} = \frac{w_o + \frac{w'}{2}}{w_o + \frac{w'_o}{2}} = \frac{w_o + \frac{w'_1}{2}}{w_o + \frac{w'_o}{2}} + \frac{\frac{w'_2}{2}}{w_o + \frac{w'_o}{2}}$$

When $\frac{c'_1}{2} \parallel \frac{c'_o}{2}$ and $\frac{c'_1}{2} \sim \frac{c'}{2}$ we may put

$$\frac{w_o + \frac{w'_1}{2}}{w_o + \frac{w'_o}{2}} = \frac{c_o + \frac{c'}{2}}{c_o + \frac{c'_o}{2}}$$

and

$$\frac{w'^2}{2} = \frac{c'}{2} \Delta i \frac{w_o + \frac{w'}{2}}{c}$$

or

$$\frac{\frac{w'^2}{2}}{w_o + \frac{w'_o}{2}} = \frac{c'}{2c} \Delta i \frac{w_o + \frac{w'}{2}}{w_o + \frac{w'_o}{2}} = \frac{c'}{2c} \Delta i \frac{1}{b}$$

Finally the last equations yield:

$$b = \frac{w_o + \frac{w'_o}{2}}{w_o + \frac{w'}{2}} = \frac{1 + \frac{c'_o}{2c_o}}{1 + \frac{c'_o}{2c_o}\frac{c'}{c'_o}} \left(1 - \Delta i \frac{c'}{2c}\right) \qquad (12)$$

Putting $b = 1$ in equation (9) and $\Delta i = \frac{k\lambda^2}{x^2+\lambda^2}$ in equations (9) and (12) as first approximation from (10'), we can define b by means of the first two equations. The thus obtained b value inserted in (10') and the numerator and denominator of the latter developed according to k and $(1 - \eta_i)$, in which both quantities may be considered as being of the same order, then obtains to

$$\Delta i = \frac{k\lambda^2}{x^2+\lambda^2} \frac{\eta_i x^2 + \lambda^2}{\eta_i x^2 + p(1-\eta_i)\lambda x + \lambda^2} \left[1 - k\lambda\frac{x}{x^2+\lambda^2} - (1-\eta_t)\frac{x^2}{\eta_i x^2+\lambda^2}\right] \qquad (10'')$$

(the terms of the second and higher order being neglected.)

For the case of zero load factor of blade element (or $\eta_i = 1$), its change in angle of flow becomes

$$\Delta i_g = \frac{k\lambda^2}{x^2 + \lambda^2} \left[1 - k\lambda\frac{x}{x^2 + \lambda^2}\right] \qquad (10''a)$$

(change in angle after neglecting the induced additive velocities, which may be expressed as geometrical change in angle.)

But Δi drops considerably from this value with the load rating (fig. 5) which indicates that the angular change is reduced by the autorotation. From this it is seen that highly loaded propellers are less sensitive to sideslip. Figure 5 shows, aside from the Δi curves defined from (10''), those accurately computed according to (8'), (9') and (12) at $k = \pm 0.2$ for different λ_x as parameter versus η_i, (λ_x = coefficient of advance at radius x). It becomes manifest that the exact Δi values are subordinate and become greater only by higher load rating.

Now it should be of interest to examine more closely the distribution of the induced additive velocities due to sideslip u_q. To this end it is assumed that the angular change Δi is, in first approximation equal to the geometrical, i.e., to the neglected induced additive velocities

$$\Delta i_g = \frac{k\lambda^2}{x^2 + \lambda^2}\left[1 - k\lambda\frac{x}{x^2 + \lambda^2}\right]$$

Then, when expressing the corresponding velocity components as $w'_s = w' - w'_o$, $u'_s = u' - u'_o$

and

$$c'_s = \sqrt{w'^2_s + u'^2_s}$$

and approximately put:

$$w'_s = \frac{x}{\sqrt{x^2 + \lambda^2}}\, c'_s, \qquad u'_s = \frac{\lambda}{\sqrt{x^2 + \lambda^2}}\, c'_s$$

and

$$w'_o = \frac{x}{\sqrt{x^2 + \lambda^2}}\, c'_o, \qquad u'_o = \frac{\lambda}{\sqrt{x^2 + \lambda^2}}\, c'_o$$

equation (9) yields:

$$\frac{c'_s}{c'_o} = \frac{w'_s}{w'_o} = \frac{u'_s}{u'_o} = pk\frac{\lambda^2}{x^2 + \lambda^2}\left[1 + k\lambda\frac{x}{x^2 + \lambda^2}\right] \qquad (9a)$$

The last equations give a clear picture of the distribution of the induced additive velocities in the plane of the blade due to sideslip. Their ratio to the corresponding induced velocities of the propeller in axial air flow, i.e. when $u_q = 0$ and $w = w_o$, diminishes considerably with the radius after having reached the maximum in the vicinity of $x = \lambda$. The distribution over the periphery is in first approximation conformably to a sine curve.

The total thrust and the torque are scarcely changed in their mean value by the yawing position of the propeller, and can be computed according to the usual method of the propeller theory. The two values increase in the half of the plane of the blade where $k = \tan \varphi \sin \vartheta$ is positive and decrease in the other half, so that the mean value remains practically constant and equal to the propeller in axial air flow of w_o velocity and with the same revolutions. On the other hand, the center of gravity of the thrust is, under these circumstances, no longer in the propeller axis, as result of which a yawing moment perpendicular to the axis of rotation is set up with respect to the propeller axis. Simultaneously there is a mean transverse force, perpendicular to the propeller axis, as a result of the unsymmetrical distribution of the tangential forces over the periphery.

The position of the resultant thrust which, moreover, is counted parallel to the propeller axis, is defined by coordinates of its intersection with the plane of the blade:

$$\left.\begin{aligned} X_o &= \frac{\int_0^{2\pi} \int_0^{1} dS \times R \sin \vartheta}{\int_0^{2\pi} \int_0^{1} dS} \\ Z_o &= \frac{\int_0^{2\pi} \int_0^{1} dS \times R \cos \vartheta}{\int_0^{2\pi} \int_0^{1} dS} \end{aligned}\right\} \qquad (13)$$

The transverse force components are:

$$\left.\begin{aligned} Q_x &= \int_0^{2\pi}\int_0^1 dT \cos\vartheta \\ Q_z &= \int_0^{2\pi}\int_0^1 dT \sin\vartheta \end{aligned}\right\} \qquad (14)$$

In equations (1') and (2'), η'_α and η'_i can be replaced by their mean values η_α and η_i and considered as being equal to the respective quantities of the propeller in axial flow (constant over the periphery). It is, namely:

$$\frac{\eta'_\alpha}{\eta_\alpha} = b = \frac{w_o + \frac{w'_o}{2}}{w_o + \frac{w'}{2}}$$

wherein b becomes smaller or greater than 1, according to whether k is positive or negative and, for the rest, deviates only at large k values and in the neighborhood of the hub more appreciably from 1. This also holds for η_i.

Thus the replacement of Δi in (1') and (2') by equation (10') reveals that

$$\int_0^{2\pi}\int_0^1 dS \times R \cos\vartheta = 0$$

and

$$\int_0^{2\pi}\int_0^1 dT \cos\vartheta = 0$$

i.e., that the resultant of the thrust intersects the plane of the blade on the X axis (fig. 1) and that the transverse force of the propeller lies on the Z axis. The vectors of the yawing moment and of the transverse force therefore coincide with the Z axis.

Developing the other two equations (13) and (14), omitting the small terms of second and higher order and integrating according to ϑ, then results in:

Yawing moment of propeller:

$$M = SX_o = \frac{1}{2} R^2 q_o \frac{\tan\varphi}{\lambda} \int_o^1 \frac{c_a z t}{\eta_\alpha} \; x\sqrt{x^2 + \lambda^2}$$

$$\times \left[\eta_\alpha + \eta_i \frac{x^2}{x^2 + \lambda^2} - \epsilon\lambda \frac{x}{x^2 + \lambda^2} + \right.$$

$$\left. + p\lambda^2 \frac{\frac{\eta_i}{\lambda}(2\eta_i - 1)x^3 - \epsilon(2\eta_i - 1)x^2 + \eta_i\lambda x - \epsilon\lambda^2}{(x^2 + \lambda^2)(\eta_i x^2 + p(1 - \eta_i)\lambda x + \lambda^2)} \right] dx \tag{15}$$

wherein S = mean thrust, and the transverse force:

$$Q = \frac{1}{2} R^2 q_o \frac{\tan\varphi}{\lambda} \int_o^1 \frac{c_a z t}{\eta_\alpha} \sqrt{x^2 + \lambda^2}$$

$$\times \left[\lambda \frac{x}{x^2 + \lambda^2} + \epsilon\left(\eta_\alpha + \eta_i \frac{x^2}{x^2 + \lambda^2} \right) + \right.$$

$$\left. + p\lambda^2 \frac{\frac{\epsilon}{\lambda}\eta_i(2\eta_i - 1)x^3 + (2\eta_i - 1)x^2 + \epsilon\eta_i\lambda x + \lambda^2}{(x^2 + \lambda^2)(\eta_i x^2 + p(1 - \eta_i)\lambda x + \lambda^2)} \right] dx \tag{16}$$

To make the formulas clearer we insert

$$\lambda_x = \frac{\lambda}{x}$$

$$\eta_i = \frac{\lambda_x}{\lambda'_x} \qquad \eta_\alpha = \frac{\lambda_x}{\lambda'_x} \frac{\sqrt{1 + \lambda'^2_x}}{\sqrt{1 + \lambda_x^2}}$$

$$c_m = \frac{M}{R^2 \pi q R} \qquad c_q = \frac{Q}{R^2 \pi q}$$

and

$$\frac{q_o}{q} = \frac{\rho \frac{w_o^2}{2}}{\rho \frac{w^2}{2}} = \cos^2\varphi$$

with λ'_x = geometrical and λ = induced coefficient of advance on peripheral radius x and c_m = yawing moment and c_q = transverse force coefficient.

Therefrom follows:

$$c_m = \Phi \sin 2\varphi \tag{15'}$$

$$c_q = \psi \sin 2\varphi \tag{16'}$$

where

$$\Phi = \frac{1}{4R\pi} \int_0^1 c_a z t \frac{\lambda'_x}{\lambda_x} \frac{1}{\sqrt{1+\lambda'^2_x}} \left[\frac{1+\sqrt{1+\lambda_x^2}\sqrt{1+\lambda'^2_x}}{\lambda'_x} - \epsilon + p \frac{(1-\epsilon\lambda'_x)\left(\lambda_x^2 + \frac{2\lambda_x - \lambda'_x}{\lambda'_x}\right)}{1+p(\lambda'_x - \lambda_x)+\lambda_x\lambda'_x} \right] x\,dx \tag{15''}$$

$$\psi = \frac{1}{4R\pi} \int_0^1 c_a z t \frac{\lambda'_x}{\lambda_x} \frac{1}{\sqrt{1+\lambda'^2_x}} \left[1 + \epsilon \frac{2+\lambda_x^2}{\lambda'_x} + p \frac{(\lambda'_x + \epsilon)\left(\lambda_x^2 + \frac{2\lambda_x - \lambda'_x}{\lambda'_x}\right)}{1+p(\lambda'_x - \lambda_x)+\lambda_x\lambda'_x} \right] dx \tag{16''}$$

Note, that c_a, ϵ and $p = \frac{c'_a}{c_a}$ ($c'_a = \frac{dc_a}{di}$, i = angle of attack of profile in radians) are for infinite span.

The last two equations offer a basis for the examination of propeller energy and for its dynamic effect under practically any likely running condition.

With the present system of coordinates (figs. 1 and 2) a propeller rotating with velocity w at an angle to its axis and with angular velocity ω is subjected to the following forces: a thrust in the Y axis (axis of rotation) con-

trary to axial component w_o and a transverse force in the Z axis in direction of the transverse component u_{q_o} of the velocity of air flow, a torque about the Y axis contrary to rotation ω (and equal to the engine torque) and a yawing moment about the Z axis, both - viewed contrary to velocity components w_o and u_{q_o} - in the same effective direction. Thrust and torque are, as already shown, scarcely dependent upon φ when the axial component of w_o and ω remain constant, and equivalent for the propeller in axial flow. These two principal forces are readily computed.*

The transverse force like the yawing moment is dependent on the angle of attack of the propeller, in addition to being largely interdependent with all its parameters, that is, with the blade form and characteristics of the blade profiles, the coefficient of advance and loading and its course over the radius. These quantities being defined in the design for normal coefficient of advance, the desired forces are readily obtained by graphic integration from (15") and (16"). It is merely necessary to write the λ'_x values in the respective formulas, which correspond to the propeller load curve corrected with $K = f\,[R(1 - x), z, \sin)\beta']$, to insure "finite number of blades." (Reference 3.) For studies of propellers under operating attitudes at other coefficients of advance, (reference 4) Troller's graphic method for propeller polars is of advantage. He uses an auxiliary diagram (fig. 6) which shows the $\frac{c_a z t}{xR}$ values for different λ_x as parameter versus angle $\beta'_x = \text{arc tan } \lambda'_x$. The basis of this diagram is the formula

$$\frac{c_a z t}{xR} = 8\pi \frac{\lambda'_x (\lambda'_x - \lambda_x)}{\sqrt{1 + \lambda'^2_x}\,(1 + \lambda_x \lambda'_x)}$$

from the general propeller theory.

Putting $\frac{dc_a}{di}$ = constant, which is acceptable for practically all profiles in the usual angle of attack range,

---

*See reports cited here as well as others by Th. V. Bienen, Th. v. Karman and Th. Troller.

and tracing $\left(\frac{c_a z t}{xR}\right)_o$ corresponding to normal operating attitude in the graph, a straight line at slope

$$\frac{d\left[\frac{c_a z t}{xR}\right]}{d\beta'_x} = \frac{dc_a}{di}\,\frac{zt}{xR}$$

can be drawn through this point, on which the $\frac{c_a z t}{xR}$ value of all other operating attitudes lies. Even the exact $[c_a = f(\beta'_x)]$ curves of the respective profiles can be traced for this purpose into the diagram in the $\frac{zt}{xR}$ scale. Then we define through the intersection of the particular λ_x line and the straight line $\left(\text{or } \frac{c_a z t}{xR}\right)$ curves the corresponding β'_x and λ'_x value. To account for the "finite number of blades" the ordinates of the straight lines and $\frac{c_a z t}{xR}$ curves are multiplied by factor $K = f[R(1 - x), z, \sin \beta'_x]$, after which the β'_x and λ'_x values corresponding to the given λ_x can be read on the abscissa. In this manner the necessary λ'_x, c_a, $\left(p = \frac{c'_a}{c_a}\right)$ and ϵ values are readily obtainable for any operating attitude.

An example will illustrate the magnitude of the yawing moment and transverse force with a certain propeller as well as the shortest method of calculation:

The dimensions of a propeller for a high-speed airplane are:

Outside diameter	D = 2.50 m
Mean load factor	σ = 0.20
Normal coefficient of advance	λ = 0.312 $V/nD = .986$
Produced thrust	S = 290 kg
At flight altitude	H = 3,000 m
With flight speed	w = 290 km/h 180 m.p.h.
Engine power, sea level	N = 650 hp
Revolutions	n = 1,980 r.p.m.

The propeller was designed according to the Bienen-v. Karman method under the assumption of optimum thrust grading with a view to friction and finite blade number. The blade profile characteristics, constant across the whole radius, are:

$c_a = 0.80, \quad \frac{dc_a}{di} = 4.9, \quad p = \frac{c'_a}{c_a} = 6.10, \quad \epsilon = 0.02$

TABLE I.

λ	x= r/R	.28	.36	.48	.60	.72	.905	Φ	Ψ
	$c_a z t(m)$	.394	.400	.400	.359	.288	.158		
	λ_x	1.115	.866	.650	.520	.433	.345		
	λ'_x	1.290	.991	.740	.589	.488	.382		
.312	$\frac{d\Phi}{dx}$	.0295	.0470	.0775	.100	.111	.090	.063	.0685
	$\frac{d\Psi}{dx}$	.0975	.0950	.0880	.0740	.0560	.0285		
	$c_a z t(m)$	.180	.175	.180	.170	.153	.0883		
	λ_x	1.43	1.11	.834	.666	.555	.442		
	λ'_x	1.53	1.175	.879	.700	.585	.463		
.40	p	13.10	13.95	13.60	12.95	11.53	10.95	.043	.066
	ϵ	.037	.040	.039	.037	.033	.031		
	$\frac{d\Phi}{dx}$	.0196	.031	.0305	.0672	.0772	.0620		
	$\frac{d\Psi}{dx}$	.0940	.0910	.0845	.0720	.0555	.0280		
	$c_a z t(m)$	.564	.570	.558	.476	.378	.210		
	λ_x	.893	.695	.521	.417	.347	.276		
	λ'_x	1.107	.854	.630	.500	.421	.328		
.25	p	3.34	3.34	3.43	3.96	4.0	4.0	.079	.064
	ϵ	.027	.027	.023	.020	.020	.020		
	$\frac{d\Phi}{dx}$	.0365	.0545	.0945	.123	.139	.117		
	$\frac{d\Psi}{dx}$	.0900	.0885	.0830	.0705	.0550	.0290		

Table I demonstrates a suitable calculation scheme. The calculation was also made for other operating attitudes ($\lambda_1 = 0.25$ and $\lambda_2 = 0.40$). It is seen that whereas the coefficient of the transverse force changes very little with the operating attitude, that of the yawing moment increases considerably at small coefficients of advance.

For the normal $\lambda = 0.312$

$$c_m = 0.063 \sin 2\varphi$$

and

$$c_q = 0.0685 \sin 2\varphi$$

or a yawing moment

$$M = R^3 \pi q \, c_m = 39 \text{ kg/m}$$

and a transverse force

$$Q = R^2 \pi q \, c_q = 34 \text{ kg}$$

for $\varphi = 10^\circ$ and the prescribed operating conditions of the propeller.

The thrust is shifted along axis X by the fraction of radius

$$X_o = \frac{r}{R} = 13.5 \text{ per cent}$$

and the ratio of transverse force to thrust is

$$\frac{Q}{S} = 11.7 \text{ per cent}$$

For comparison we have compiled in Tables II, III, and IV, and in Figures 7 and 8 the results of the experiments (reference 5) made in the National Physical Laboratory, together with figures obtained from equations (16') and (16"). The model was a four-blade propeller with $D = 0.305$ m diameter and normal coefficient of advance $\lambda = 0.235$ and $\sigma = 0.365$ load rating. Blade width, profile characteristics and coefficient of advance over the radius are given in Table II.

TABLE II.

J	λ	x = r/R	.15	.30	.60	.90	ψ
		c_a zt(m)	.108	.117	.111	.061	
		λ_x	1.568	.784	.392	.261	
		λ'_x	2.05	.922	.470	.310	
.739	.235	p	3.50	4.75	6.50	6.95	.0725
		ϵ	.060	.042	.032	.025	
		$\frac{d\psi}{dx}$	.077	.097	.086	.0433	
		c_a zt(m)		.0690	.0695	.0411	
		λ_x		1.00	.50	.333	
		λ'_x		1.102	.543	.362	
.943	.30	p		8.05	10.55	10.30	.071
		ϵ		.056	.037	.038	
		$\frac{d\psi}{dx}$		.093	.087	.0437	
		c_a zt(m)		.164	.151	.077	
		λ_x		.60	.30	.20	
		λ'_x		.779	.4075	.267	
.565	.18	p		3.39	4.77	5.50	.080
		ϵ		.059	.030	.035	
		$\frac{d\psi}{dx}$		.1055	.0925	.049	

TABLE III.

φ°		5	10	15	20	25
Calculated $\lambda = 0.235$	c_q	.0126	.0248	.0362	.0466	.0556
	λ	.244	.226	.222	.217	.213
Measured	c_q	.0136	.0246	.0356	.0470	.0587

TABLE IV.

Calculated	$\bar{V}$	,565		,739		,943		
	λ	.18		.235		.30		
	ψ	.080 .0392		.0725 .0356		.0710 .0348		
Measured at $\varphi = 10^\circ$	λ	.150	.171	.187	.203	.226	.247	.278	.292
	ψ	.0955	.0860	.0815	.0755	.0720	.0705	.0670	.0730

The comparison shows close agreement between our formulas and the experimental data. Table III and Figure 7 show the c_q values for $\lambda = 0.235$. Although the measurements did not exactly obtain to this figure for λ, it nevertheless was not necessary to correct the data, because the coefficient of transverse force in this range is practically unaffected by λ. (Fig. 8). When it is noted that our experiments were confined to small k values ($\tan\varphi < 1$) the ambit of agreement appears abundant, the more so, since according to Figure 7, the discrepancies of the theoretical curve from the true attitude will not be abnormally large even above $\varphi = 25^\circ$.

The calculated and measured ψ values for variable coefficient of advance λ are compiled in Table IV. The ψ values determined from (16") were arrived at from the data in Table II and Figure 6, whereas the test data were extrapolated conformably to (16'). These data are plotted against λ in Figure 8 on the theoretically defined points.

The load curve $\sigma = \frac{S}{R^2 \pi q}$ evaluated from the measurements

is also given for comparison.

It is manifest that the change in proportionality factor ψ of the transverse force for a given propeller of stated shape and dimensions with λ is insignificant, as moreover, is readily seen from (15") and (16"). For certain propeller dimensions the lift coefficient of the blade profiles becomes lower by increased λ, and $p = \frac{c'_a}{c_a}$ correspondingly greater and vice versa. It follows from this, that when disregarding the inferior effect of the change in ϵ and $\frac{\lambda'_x}{\lambda_x}$, the proportionality factor Φ of the yawing moment decreases as λ increases, whereas that of ψ remains practically constant. This fact is very significant when noting that the increase in λ is followed by a lower propeller-load factor (fig. 8) and by a markedly higher ratio of transverse force to thrust.

The very fact that c_q does not change with the coefficient of advance and consequently with the flight speed, makes it possible to demonstrate the effect of the yawing propeller on the stability of the airplane very clearly.

Assume, in place of the propeller, an airfoil of symmetrical profile is rotatably disposed about the propeller axis, that is, in such a way as to be able to automatically assume a setting perpendicular to the YZ plane (propeller axis - flight direction), and in the XY plane. Then the transverse force of the propeller can be replaced by the lift of this airfoil, provided this lift is always counted perpendicular to the propeller axis. For normal profiles in the usual range of angles, a fairly close approximation gives the lift coefficient as

$$c_a = \alpha \sin 2\varphi \quad (\alpha = \text{constant})$$

with φ = angle of attack, figured from the ($c_a = 0$) line. After approximating the usual geometrical profiles at $\alpha = 2$, the magnitude of this area (lift = transverse force) is

$$f_q = \frac{1}{2} t = \frac{\psi}{\alpha} R^2 \pi = \frac{\psi}{2} R^2 \pi$$

and the transverse force (lift):

$$Q = c_a f_q q$$

Expressed in this form the term lends itself readily for use in the stability equations.

Now in order to justify any general remarks about the behavior of a propeller in yaw the terms (15") and (16") must be rid of the propeller dimensions (zt and R). This is accomplished by means of equation (1), which, transformed reads:

$$\sigma = \frac{dS}{2r\pi dr\ q} = \frac{c_a z t}{2r\pi} \frac{1 + \lambda_x^2}{\lambda_x^2} \frac{1 - \epsilon\lambda'_x}{\sqrt{1 + \lambda'^2_x}}$$

or

$$c_a z t = 2\pi R x \sigma \frac{\lambda_x^2}{1 + \lambda_x^2} \frac{\sqrt{1 + \lambda'^2_x}}{1 - \epsilon\lambda'_x} \qquad (1a)$$

The last equation, written in (15") and (16"), leaves it dependent only on σ_x and λ_x and an ($p = \frac{c'a}{c_a}$ and ϵ).

Now it is readily apparent that the Φ and ψ values increase with λ_x for constant σ_x and profile characteristics ($p = c'a$ and ϵ). In other words, the ratio of the c_q and c_m values to σ_x increases enormously with λ_x under these circumstances. By constant λ_x and variable propeller loadings this ratio varies only slightly with the load rating and shows rather a tendency to drop at its increase.

For the first approximation of the propeller force an older formula of the author can be used. To integrate equation (14) over the radius the blade number was assumed infinite and the total blade width expressed by

$$zt = 8\pi R \frac{1 - \eta_i}{\eta_i^2} \frac{\lambda^2}{c_a} \frac{x^2}{(x^2 + \lambda^2)^{3/2}}$$

as function of the radius, which is equivalent to the load distribution

$$\sigma_x = 4 \frac{1 - \eta_i}{\eta_a \eta_i} \frac{x^2}{x^2 + \lambda^2}$$

$\frac{c'_o}{2\,c_o} = \frac{w'_o}{2\,u_o} = \frac{\lambda}{x}\,\frac{1 - \eta_\alpha}{\eta_\alpha}$ replaced equation (11) and η_o and η_i were kept as constant across the radius. The approximation formula reads

$$c_q = \psi_1 \sigma \sin 2\varphi$$

where

$$\psi_1 = \frac{1}{4\eta_i}\,\frac{\lambda}{1 - \lambda^2 \ln\frac{1 + \lambda^2}{\lambda^2}}\left\{\lambda\left(\ln\frac{1 + \lambda^2}{\lambda^2} - \frac{1}{1 + \lambda^2}\right) + \right.$$

$$+ \epsilon\eta_\alpha\left(2 + \lambda \arctan\frac{1}{\lambda} + \right.$$

$$\left. + \frac{c'_a}{c_a}\,\frac{2\eta_\alpha - 1}{\eta_\alpha}\,\frac{\lambda}{(1 + s^2)^2}\left[(1 + 3s^2)\arctan\frac{1}{\lambda} - \right.\right.$$

$$\left.\left. - \frac{1 + s^2}{1 + \lambda^2}(\lambda + s + \epsilon\eta_i)\right]\right\} \qquad (17)$$

and

$$s = \frac{1 - \eta_\alpha}{\eta_\alpha}\,\frac{c'_a}{c_a}$$

The mean efficiencies can be determined from

$$\eta_\alpha = \frac{2}{1 + \sqrt{1 + \sigma}}$$

$$\eta_i = \frac{2}{1 + \sqrt{1 + \sigma}}(1 - \sigma\lambda^3)$$

with σ = mean load rating.

For the example in question the formula yields

$$\psi_1 = 0.223$$

or

$$\frac{c_q}{\sigma} = 0.223 \sin 2\varphi$$

For $\varphi = 10^\circ$ angle of attack of propeller it is $\frac{c_q}{\sigma} = 7.8$ per cent against the more exact value of 11.7 per cent.

RESUME

The theoretical analysis reveals that a propeller in yaw is subject to axial thrust and torque and in addition to a transverse force and a yawing moment. The transverse force subtends the axis in the plane defined by it and the airflow direction, and acts in direction of the sideslip component u_{q_0}. The force couple corresponding to the yawing moment lies in the plane through the propeller axis and a perpendicular to this and the direction of flow, and acts, when viewed opposite to the axial and transverse velocity component, in the inverse direction of the propeller rotation. For lightly loaded propellers with high coefficient of advance, that is, in high-speed airplanes, these forces can be comparatively great, and thereby affect appreciably the airplane stability and flight conditions during climb and banking.

The transverse force may be assumed replaced by the lift of an airfoil disposed perpendicular to the flow direction of dimensions $l\ t = \left(\frac{\psi \sin 2\varphi}{c_a} R^2 \pi\right)$, whose $(c_a = 0)$ line is coincident with the propeller axis. This representation reveals very clearly the relation between the transverse force of the propeller and the effect of the tail surfaces and their effect on the stability of the airplane.

This effect is particularly important in airplanes

with propellers mounted far ahead (or back) of the center of gravity. The computed axial thrust and torque undergo no perceptible change in mean value for the propeller in yaw, although its variation about the mean value which is of the order of magnitude of the transverse force and synchronized with the rotative speed, may induce dangerous blade flutter as well as vibrations in the whole propeller-engine unit.

II. EXPERIMENTS ON THE EFFECT OF THE SLIPSTREAM ON THE CONTROL SYSTEM OF AN AIRPLANE

Part I of this report describes the phenomena produced in the plane of the blade as result of the yaw of the propeller against the flow and relative flight direction. It was proved that thereby the air forces acting on the propeller can momentarily be changed materially.

Accordingly the flow pattern aft of the propeller will also be different, so that the air forces on the parts of the airplane within the slipstream can be appreciably affected. Ordinarily the mean direction of the developed slipstream, even apart from the spiral, deviates from the flow direction and alters, above all, the effective mean flow angle of the affected surfaces. But the flow picture is very complex and not very readily amenable to analysis.

So in order to obtain a clear picture of the slipstream form and particularly of its influence on the controls, we explored the flow behind the propeller and its effect on a fin by experiment.

1. Test Arrangement and Method

The experiments were made on the propeller torque stand in the wind tunnel of the Aachen Aerodynamic Institute.

The model propeller (D = 0.40 m diameter, fig. 9) was driven from an electric motor mounted on a post rotatable about two mutually perpendicular axes (figs. 10 and 11). The propeller axis was turned in the vertical plane against the flow direction. To minimize flow disturbances, we re-

sorted to fairings. (See fig. 10.) The propeller revolutions were recorded by stroboscope. The thrust was recorded in axial direction by a suitable diaphragm or thrust metering box. The instrument for recording the speed in magnitude and direction is shown in Figures 12 and 13. The static pressure gauge A is rotatable about two mutually perpendicular, axes meeting in the test point, so that the position of the test point remains unchanged. The opposite static tubes of the instrument are connected to U tubes B. When the axis of the static pressure gauge is coincident with the velocity direction the static pressures in one pair of tubes equal that in the other pair. Then, when the U tubes are set to zero, by turning the instrument, the angles formed by the air velocity with two mutually subtended planes can be read on disk C and plate D which are marked off in degrees and vernier division. The zero position on both degree divisions is determined in the same way by stopped propeller. The sensitivity of the test apparatus for angle changes can be regulated as desired by using more or less sloping U tubes. For speed quantity measurements the inner, shielded tube is connected with one of the outside to a manometer.

For investigating the slipstream effect on a ⓢwing within its range, a fin with symmetrical profile of 600 mm span, 200 mm chord and 20 mm thickness was horizontally suspended on the test balance, so that the leading edge of the fin intersected the propeller axis at right angle, 1.10 m distant from the plane of the blade. The air loads on the fin were measured with suitable diaphragm boxes.

The measurements were made for different angles of attack of the propeller axis against the air flow direction, i.e., $\varphi = 0^\circ$, 5°, 10° and 15°, constant $n = 2{,}500$ r.p.m. and two air flow velocities corresponding to $q = 7.5$ and 15 kg/m^2 dynamic pressure, the axis being turned in the vertical plane. Magnitude and direction of the velocity in the slipstream was measured with the above described instrument in three successive cross sections parallel to the plane of rotation at $z = 0.11$, 0.58 and 1.16 m distance from the latter, that is, along one axis lying in the vertical plane and one perpendicular to this in the stream center. The instrument was carried in these two directions, as seen in Figure 14, and was adjustable parallel to the flow direction by means of a tube. The center of the stream could be accurately defined with the static pressure gauge, because of its quick reaction to the sudden directional changes in velocity in this point. When the instru-

ment in the center itself is set parallel to the vortex axis, the manometer columns return to zero setting for reasons of symmetry and give very severe deflections even when only minutely displaced from its position.

2. Results of Tests

The primary object of the measurements was to gain an insight into the form of flow behind a propeller. The results are shown in Figures 15 and 16 for two running conditions. The velocities parallel to the stream center line are plotted against the distance from the stream center. The center line is defined by the center points in the individual cross sections and shows at the same time the mean direction of the propeller slipstream. The slipstream remains, independent from the angle of attack of the propeller, approximately cylindrical, and its boundary with the distance from the plane of the blade becomes only little indistinct because of friction. The jet contraction is only slightly perceptible directly behind the propeller, after which the slipstream slightly diverges again.

The air speed in the plane of the blade is the resultant of inflow and induced velocity. As shown in Part I, the air forces of the blade elements and as a result thereof the induced as well as the total velocities for the propeller in yaw are unsymmetrically distributed over the periphery. The phase of this distribution is shifted by the autorotation of the vortex system with the distance from the plane of the blade in relation to the radius and rate of slipstream rotation in the direction of rotation of the propeller. This likewise alters the velocity distribution across the radius with respect to the distance from the plane of the blade.

The mean direction of the slipstream is defined as follows: the propeller experiences, aside from the mean axial thrust (leaving out the torque), a force component perpendicular to this, which in the present case is upward in the vertical plane. Accordingly the air quantity traversing the plane of the blade is accelerated in both force directions. The resultant mean air speed in the slipstream is therefore geometrically composed of the additive velocities corresponding to air flow velocity and the cited forces. Figure 17; the slipstream direction is graphically shown for both running conditions with the respective $\varphi = 5^{\circ}$, 10° and 15°.

The transverse force for the model, computed according to the known method, was

$$c_q = \frac{Q}{R^2 \pi q} = 0.125 \sin 2\varphi$$

The mean induced additive velocity corresponding to the thrust was taken from the measurements in cross section $z = 0.11$ m behind the propeller, whereby

$$\frac{w'_q}{w'_s} = \frac{c_q}{\sigma}$$

for the other velocity component.

For $\varphi = 5^\circ$ the thus defined mean slipstream direction is in close agreement with the test data. With $\varphi = 10^\circ$ the measured angle between mean slipstream and air-flow direction is somewhat smaller, and with $\varphi = 15^\circ$ it differs considerably from the calculated value.

This discrepancy is due to the following: calculation did not allow for the fact that the propeller slipstream, when obliquely flowing into the main stream, is surrounded by the enveloping fluid. (Fig. 18.) Now there is a pressure difference on the area of discontinuity because of the probable vortex separation on the downstream side, which deflects the slipstream toward the air-flow direction. This effect is however, insignificant except at unduly large φ, so that in this range the mean slipstream direction can be quite closely approximated by the above method.

With the same working conditions of the propeller we then investigated experimentally the effect of the slipstream on the air forces directly on a fin with symmetrical profile (span: 600 mm, chord: 200 mm, thickness: 20 mm), which, conformably to the horizontal tail unit, was placed horizontally about 1.10 m behind the plane of the blade, so that its leading edge met the propeller axis.

Figure 19 shows the test data for the two operating attitudes with different φ as parameter in the $c_a = f(\alpha_f)$ diagrams, c_a being the lift coefficient referred to total fin area and air-flow velocity, and α_f the angle of attack of the fin. When the propeller axis is parallel to the air-

flow direction the slipstream also is axial and the fin is in its center. Its angle of attack, because of the slipstream rotation, increases on one side and decreases on the other in the same measure. The result is an unsymmetrical lift distribution (reference 6) about the longitudinal axis which is opposite to the propeller torque and balances it in part. The mean lift however, remains about the same as if there were no rotation in the slipstream, and it may be considered as being dependent on the axial velocity only in this case, i.e., that the fin loading increases with the induced axial velocity and the load rating of the propeller. But ordinarily, when the propeller axis slopes toward the flow direction, the mean rate of advance in the propeller slipstream also deviates from this direction, and thereby changes (that is, decreases) the effective mean angle of attack of the fin. On top of that, as φ increases the fin emerges more and more from without the slipstream, so that in our case it is no longer in contact with it when $\varphi \geq 15^{\circ}$. (Figs. 15 and 16.)

Based upon this reasoning the conditions may be briefly summed up as follows: when the propeller axis is parallel to the direction of flow the lift of the fin is increased by the increment of the rate of advance in the propeller slipstream. Turning the propeller out of this position, the lift then deviates from this value, partly because of the decreased effective mean angle of attack of the fin and partly as result of the emergence of the fin from within the range of the higher velocities. In Figure 19 this is so displayed that the rise of the lift curves $c_a = f(\alpha_f)$ decreases with φ while simultaneously being shifted parallel to the axis of the abscissa.

Another diagram traced by means of the $[c_a = f(\alpha_f)]$ diagram in Figure 19, is Figure 20, which shows the lift coefficient of the fin versus φ for different fin displacements with respect to the propeller axis α_{f_o} as parameter. Here the rise of the $[c_a = f(\varphi)]$ is seen to increase with the load rating of the propeller, i.e., that the effect of the velocity increase in the propeller slipstream predominates.

Any calculation of the air loads of a blade surface within the slipstream must first of all make due allowance for unsymmetrical velocity distribution and limited range of higher velocities, that is, of the same order of magni-

tude as the dimensions of the surface. In addition, the mean velocity far behind the propeller is lower because of the friction and its distribution is altered. For parallel position of propeller axis to direction of flow, the ratio of the mean additive velocities at distance 0.11 m and 1.16 m behind the plane of the blade is = 1.25 for $\lambda = 0.213$ and = 1.14 for $\lambda = 0.300$. The fact that the velocity distribution far behind is altogether different from that in the plane of the plate and load distribution (see figs. 15 and 16) renders it, moreover, difficult to find the interdependence between propeller loading and control surfaces. Computing the lift of the fin according to

$$A = c_a \int_0^l t\,dx\rho\,\frac{w^2}{2} \qquad (18)$$

where w = velocity far behind the propeller, yields abnormally high figures.

The ratio of mean velocity of advance in the slipstream far behind the plane of the blade to the undisturbed flow velocity is by approximation according to the propeller theory:

$$\frac{w}{w_o} = \sqrt{1 + \sigma}$$

(σ = mean load factor of propeller.) With the lift proportional to the square of the speed and the measured value for σ, equation

$$\frac{c_a}{c_{a_o}} = \left(\frac{w}{w_o}\right)^2 = 1 + \sigma \qquad (19)$$

yields

$$\text{for } \lambda = \begin{vmatrix} 0.213 \\ 0.30 \end{vmatrix} - \frac{c_a}{c_{a_o}} = \begin{vmatrix} 2.05 \\ 1.42 \end{vmatrix}$$

wherein c_{a_o} = lift coefficient of a supporting surface in undisturbed flow and c_a in the slipstream, both referred to the undisturbed flow velocity.

When extrapolating the c_a values from the plot in Figure 19, which are referred to the total fin area $l\,t$ = 600 × 200 mm, according to

$$c_{a_1} = \frac{l\,c_a - (l - D)c_{a_0}}{D}$$

(D = propeller diameter), the measurements yield with

$$\lambda = \begin{vmatrix} 0.213 - \frac{c_{a_1}}{c_0} = \\ 0.30 \quad - \end{vmatrix} \begin{vmatrix} 1.55 \\ 1.24 \end{vmatrix}$$

Here the discrepancy between the theoretical and the experimental c_a values is markedly pronounced. It is largely due to the lower mean velocity in the slipstream as result of the friction, because, when we substitute for w the mean velocity measured (on the fin) in the cross section 1.16 m distant from the plane of the plate, and when we compute the corresponding c_a values according to (18), we have with

$$\lambda = \begin{vmatrix} 0.213 - \frac{c_a}{c_{a_0}} = \\ 0.30 \quad - \end{vmatrix} \begin{vmatrix} 1.53 \\ 1.20 \end{vmatrix}$$

This shows that the air loads on a supporting surface within the slipstream are in close approximation proportional to the square of the mean velocity (referred to propeller disk area) at the particular point. However, this velocity is severely slowed up by the air friction and very differently from the theoretical, defined according to the usual propeller theory, which makes mathematical analysis of the forces difficult.

The effect of change of flow direction in the slipstream is, as Figure 19 reveals, inverse.

Assuming the angle between flow and mean slipstream direction as proportional to φ, that is:

$$\gamma = k\,\varphi$$

the effective mean angle of attack of the fin is:

$$\alpha_e = \varphi - \gamma - \alpha_{f_o} = (1 - k)\ \varphi - \alpha_{f_o}$$

and by constant velocity:

$$c_a = \text{constant},\ \alpha_e = \text{constant}\ \left[(1 - k)\ \varphi - \alpha_{f_o}\right]$$

The rise of the c_a (φ) curves is therefore diminished by the slipstream deflection in the ratio of $(1 - k)$. The emergence of the fin from without the slipstream acts in the same sense.

On the basis of the last diagram (fig. 20) it can finally be ascertained that the stability of the airplane is increased by the effect of the free slipstream on the horizontal tail surfaces and that this effect grows with the load rating of the propeller.

SUMMARY

The quantity of air which the disk area described by propeller blades travels through, is accelerated rearward conformably to the momentum of the forces acting on the propeller. This accelerated air mass forms behind the propeller the so-called slipstream, in which among others, the mean velocity of advance is increased.

If the propeller axis slopes toward the relative flight direction, the slipstream direction likewise changes, i.e., it sets up a downwash behind the propeller. It was shown how this deviation can be mathematically defined. The calculation is in close agreement with the experimental data except for abnormal slope of propeller axis to air flow direction; with appreciable slope the momentum of the slipstream is partially split up in the surrounding air because of the circulation, and the downwash of the slipstream is diminished.

A control surface attached behind the propeller finds itself in the range of higher velocities and downwash by the yaw of the propeller, which increases with the slope. The effect of the velocity increase is much more pronounced than that of the downwash, as a result of which the dynamic

effect of a horizontal tail group in the slipstream is thereby increased.

The deflection of the slipstream from the air-flow direction can, at least for small yaw, be determined from the running conditions of the propeller. But the effect of speed increase cannot be resolved with the conventional methods of airfoil theory, because the flow is very different from the uniform potential flow. Besides, the velocity in the slipstream is not only slowed up by the friction, but its distribution also is totally different at the place of the attached surface from that in the plane of the blade and the thrust grading, as result of the coiling up of the spiral vortex surfaces.

According to the formula

$$A = c_a \int_0^l t\,dx\rho\,\frac{w^2}{2}$$

Where w is, as before, the velocity far to the rear of the plane of the blade, the lift of a surface placed in the slipstream is too high. To insure the exact amount due account must be taken of this quoted slowing up and different velocity distribution on the surface together with the fact that the range of the higher velocities is of the same order of magnitude as the dimensions of the control surface.

The effect of the slipstream on the control surfaces and through it on the stability of the airplane can become comparatively great especially with highly loaded propellers, a fact which must be borne in mind in exact investigations of flight conditions and stability of airplanes. The exact determination of this effect is impossible until all the cited flow phenomena in the propeller slipstream are amenable to more precise theoretical and experimental analysis.

Translation by J. Vanier,
National Advisory Committee
for Aeronautics.

REFERENCES

1. Clarke, T. W. K.: Effect of Side Wind on a Propeller. R. & M. No. 80. British A.C.A., 1912-1913.

Harris, R. G.: Forces on a Propeller Due to Sideslip. R. & M. No. 427, British A.C.A., 1918.

2. Pistolesi, E.: Influsso di un vento laterale sul funzionamento delle eliche. L'Aerotecnica, Vol. V, No. 2, 1925. Contributo allo studio dell elica in un vento laterale. L'Aerotecnica, Vol. VI, No. 10, 1927. Nuove considerazioni su problema dell' elica in un vento laterale. L'Aerotecnica, Vol. VII, No. 3, 1928.

3. Prandtl-Betz: Schraubenpropeller mit geringstem Energieverlust. Vier Abhandlungen zur Aerodynamik.

4. Troller, Theodor: Die Konstruktion der Propellerpolaren. Z.F.M., 1929., p. 245.

5. Bramwell, F. H., Relf, E. F., and Bryant, L. W.: Experiments to Determine The Lateral Force. R. & M. No. 123, British A.C.A., 1914.

6. Leimer, A.: Der Einfluss der Propellerstrahldrehung auf die Belastung des Höhenleitwerks wurde in der Versuchsanstalt Z.A.H.I. Techn. d. Luftflotte, Moscow, experimentell untersucht. Z.A.H.I. Techn. d. Luftflotte Vol. 1, No. 1, July, 1927, pp. 63-85.

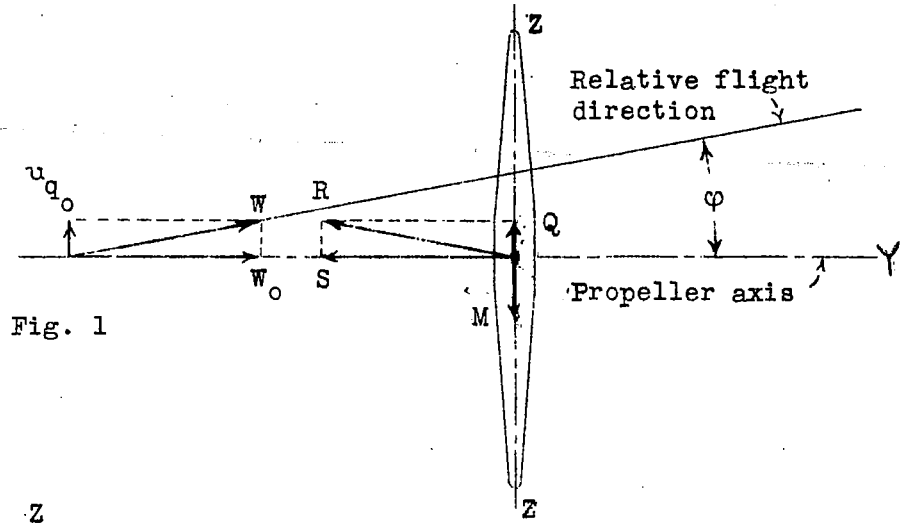

Fig. 1

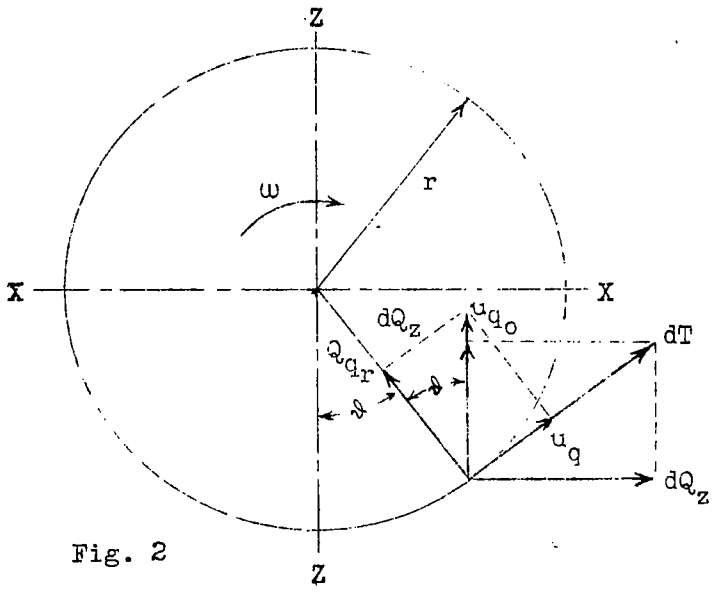

Fig. 2

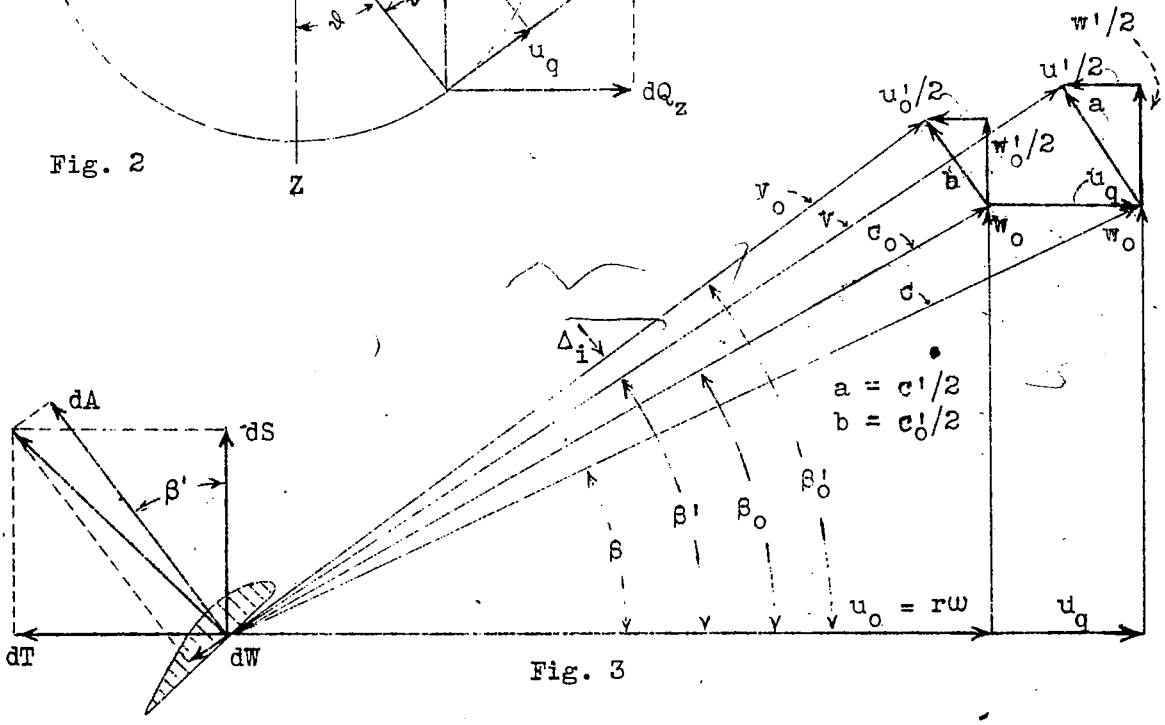

Fig. 3

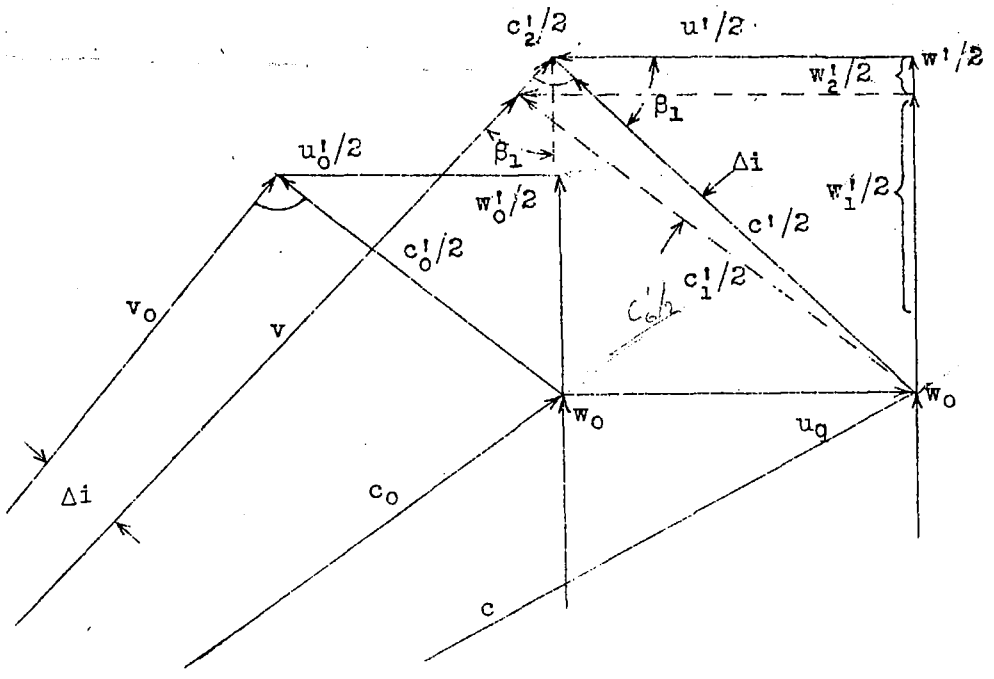
$c_2'/2$
$u'/2$
$w'/2$
$w_2'/2$
β_1
$u_0'/2$
β_1
Δi
$w_1'/2$
$w_0'/2$
$c'/2$
$c_0'/2$
$c_1'/2$
v_0
v
w_0
w_0
u_g
Δi
c_0
c

Fig.4

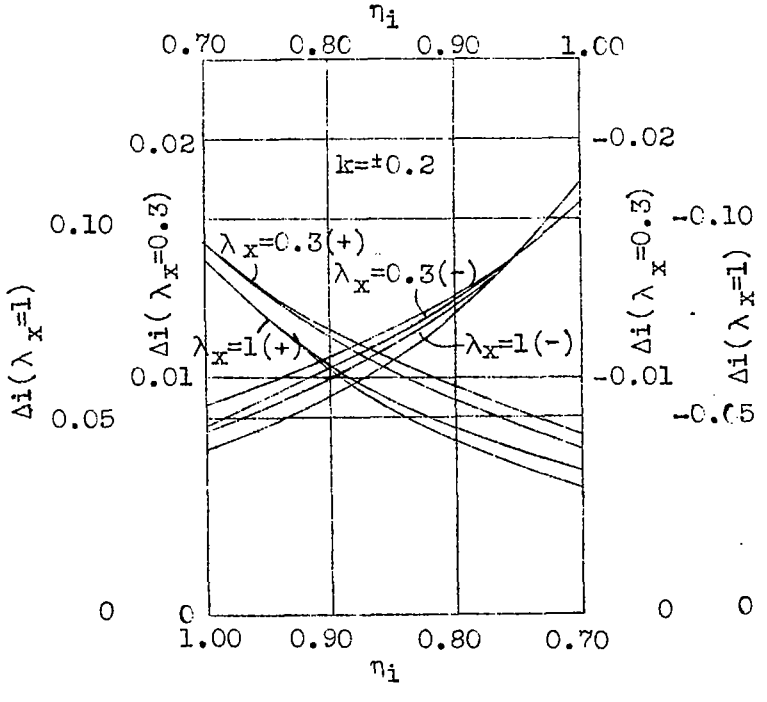
η_i
0.70
0.80
0.90
1.00
0.02
-0.02
k=±0.2
0.10
-0.10
λ_x=0.3(+)
λ_x=0.3(-)
$\Delta i(\lambda_x=0.3)$
$\Delta i(\lambda_x=1)$
λ_x=1(+)
λ_x=1(-)
0.01
-0.01
0.05
-0.05
0
0
1.00
0.90
0.80
0.70
η_i

Fig.5

Fig.6

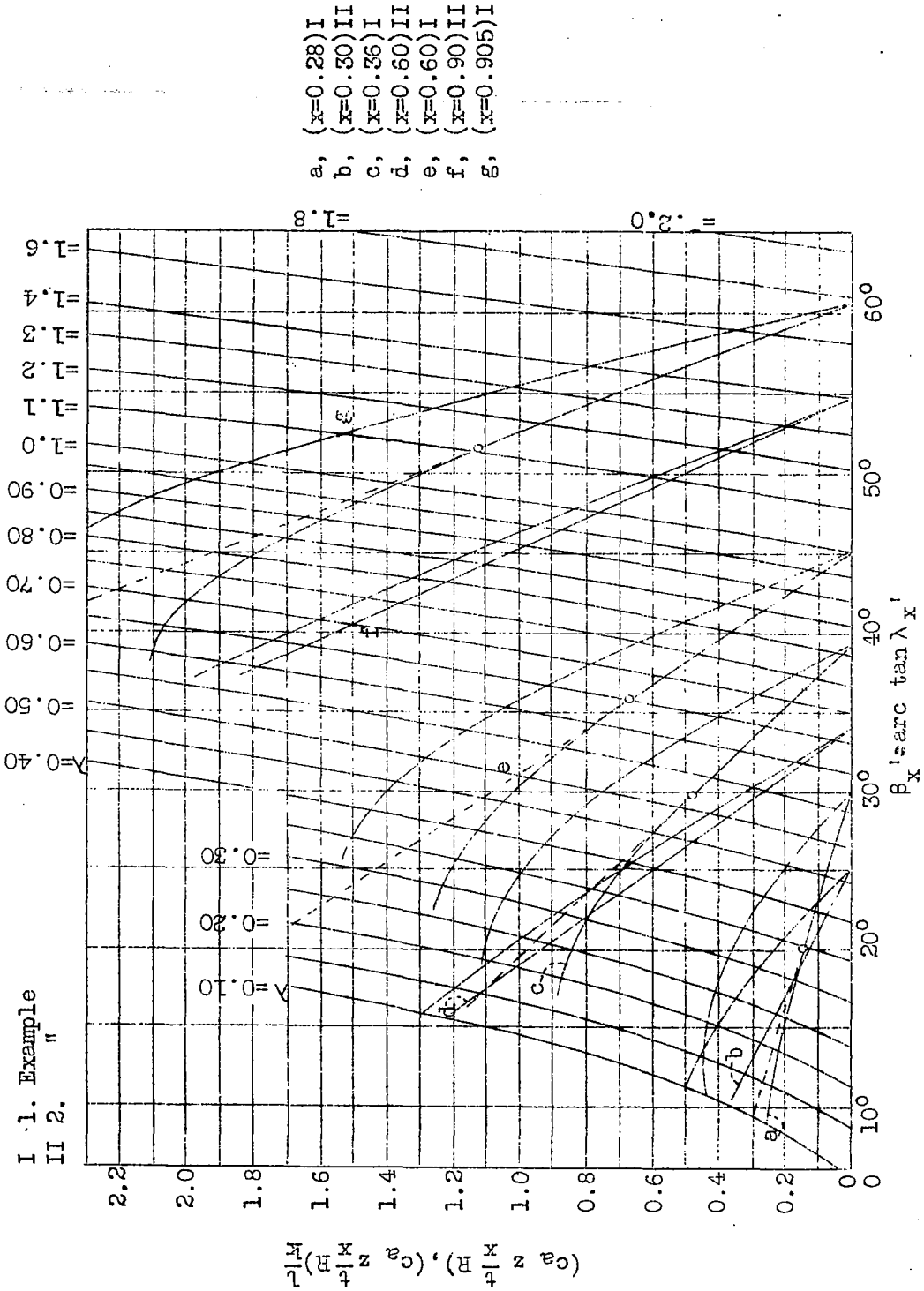
a, (x=0.28)I
b, (x=0.30)II
c, (x=0.36)I
d, (x=0.60)II
e, (x=0.60)I
f, (x=0.90)II
g, (x=0.905)I
=1.8
=2.0
=1.6
=1.4
=1.3
=1.2
=1.1
=1.0
=0.90
=0.80
=0.70
=0.60
=0.50
=0.40
λ
=0.30
=0.20
λ =0.10
I 1. Example
II 2. "
0
10°
20°
30°
40°
50°
60°
β_x = arc tan λ_x'
0
0.2
0.4
0.6
0.8
1.0
1.2
1.4
1.6
1.8
2.0
2.2
$(c_a z \frac{t}{x} R), (c_a z \frac{t}{x} R) \frac{t}{h}$

Fig.6

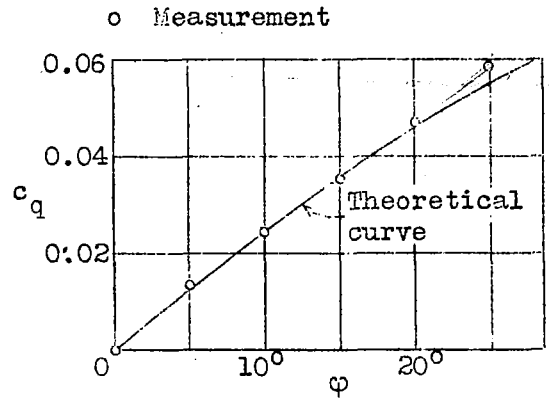

Fig.7

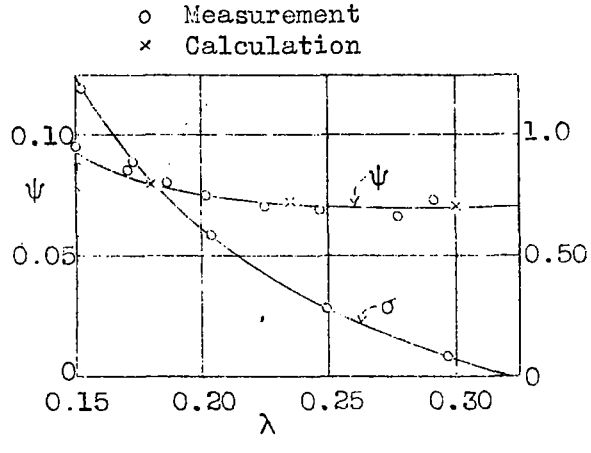

Fig.8

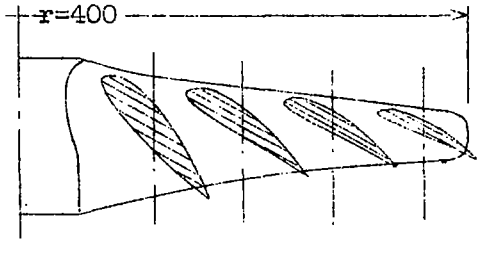

Fig.9

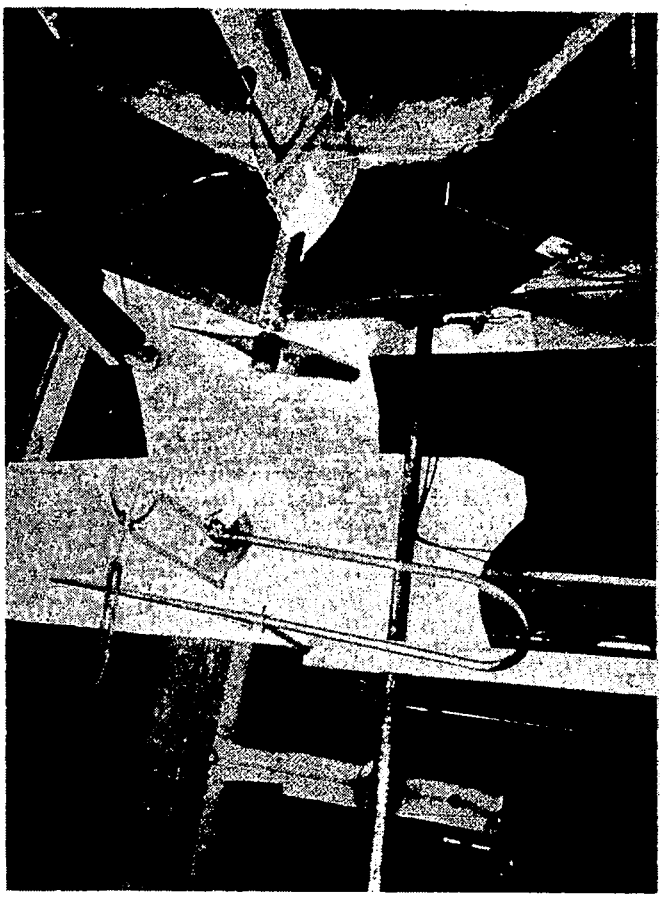

Fig. 14

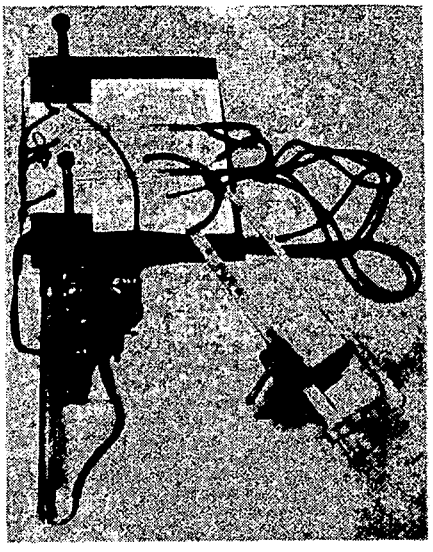

Fig. 12

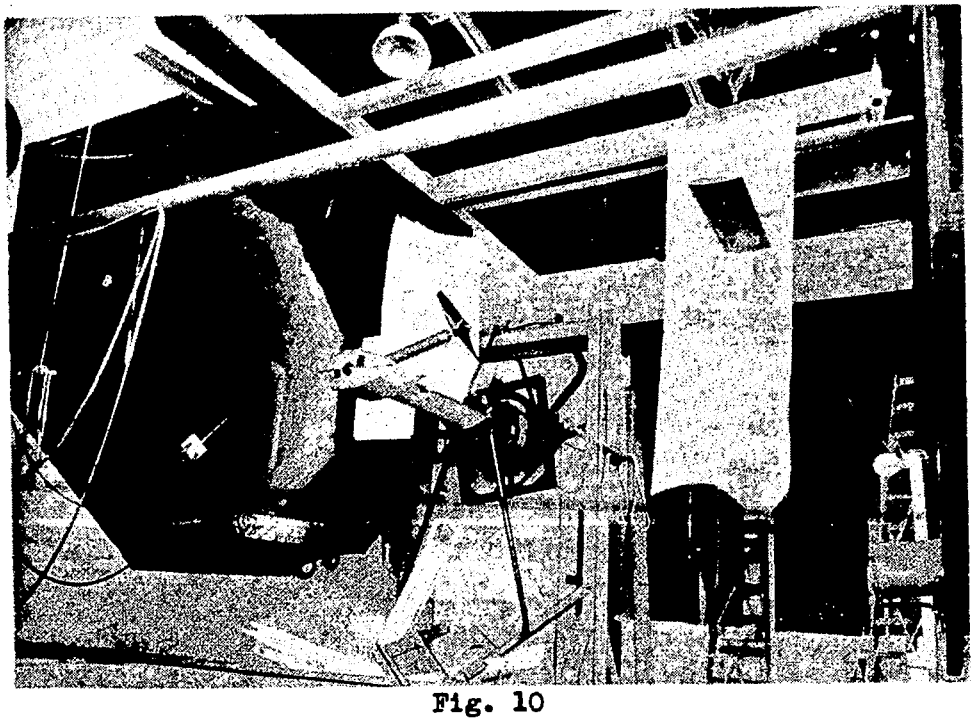

Fig. 10

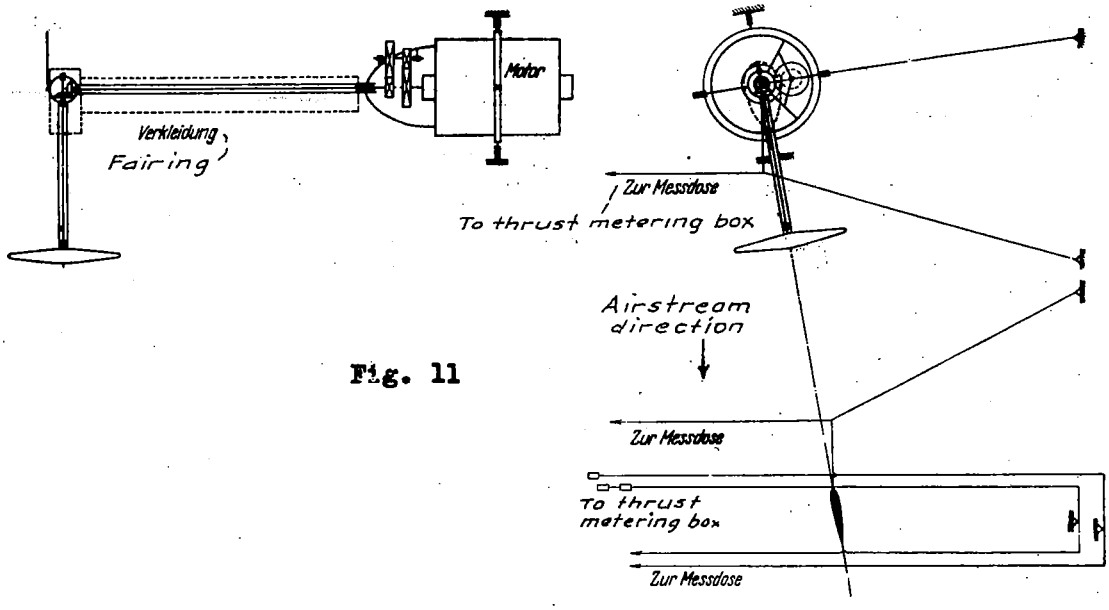

Fig. 11

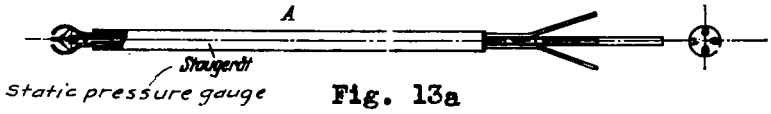

Fig. 13a

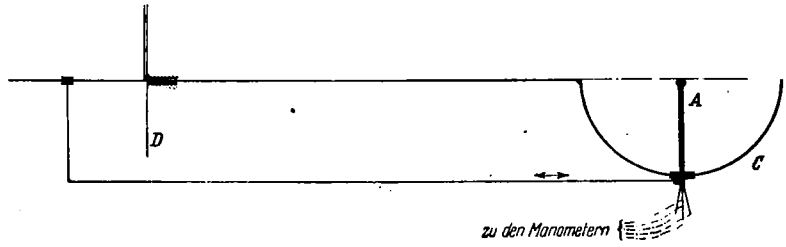

Fig. 13b

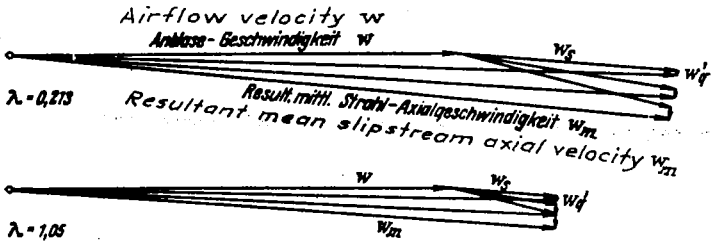

Fig. 17

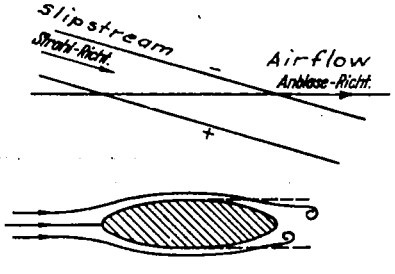

Fig. 18

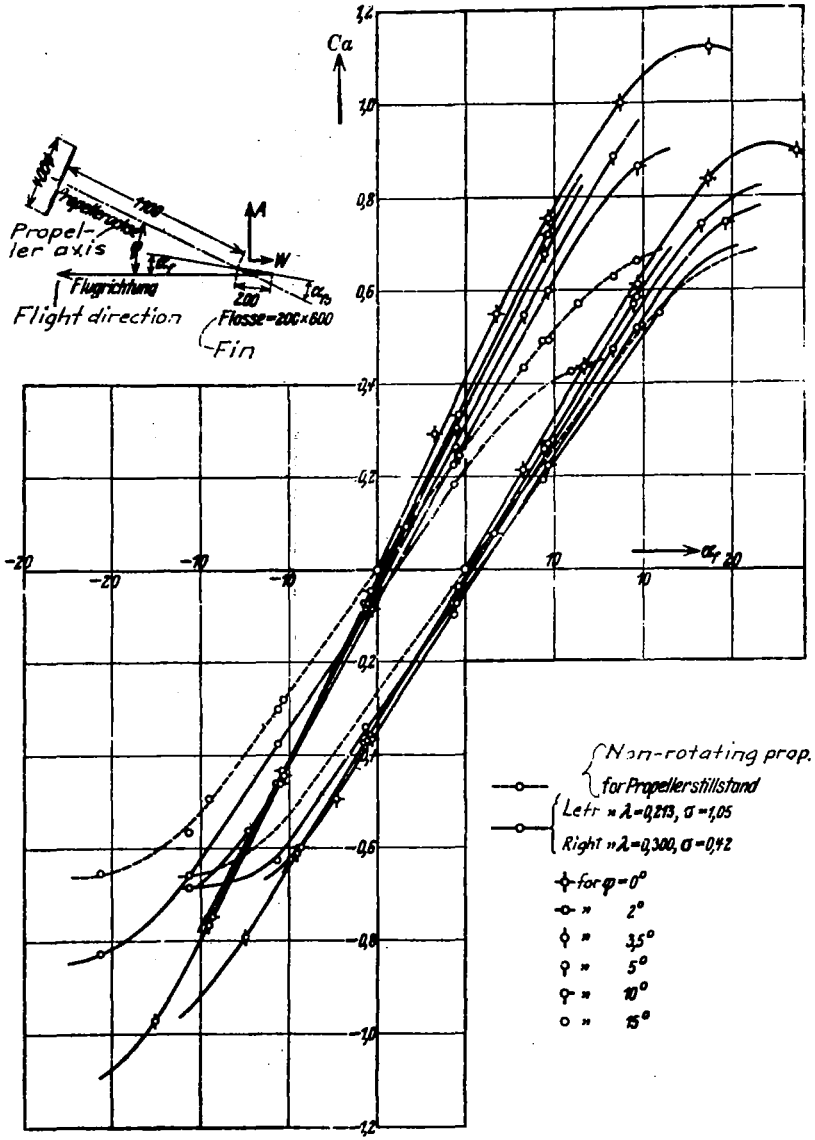

Fig.19

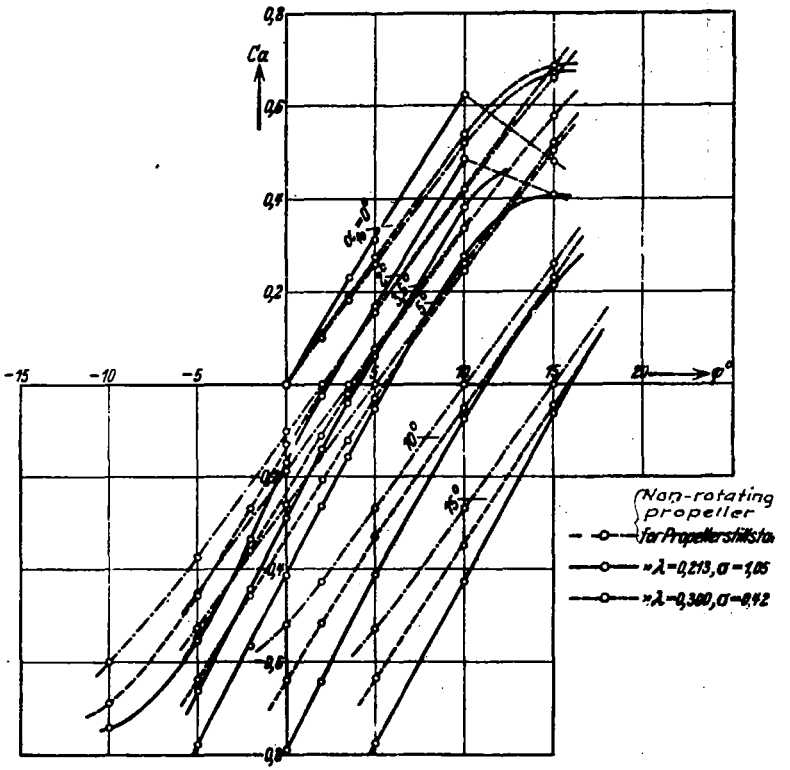

Fig.20

Figs.19,20

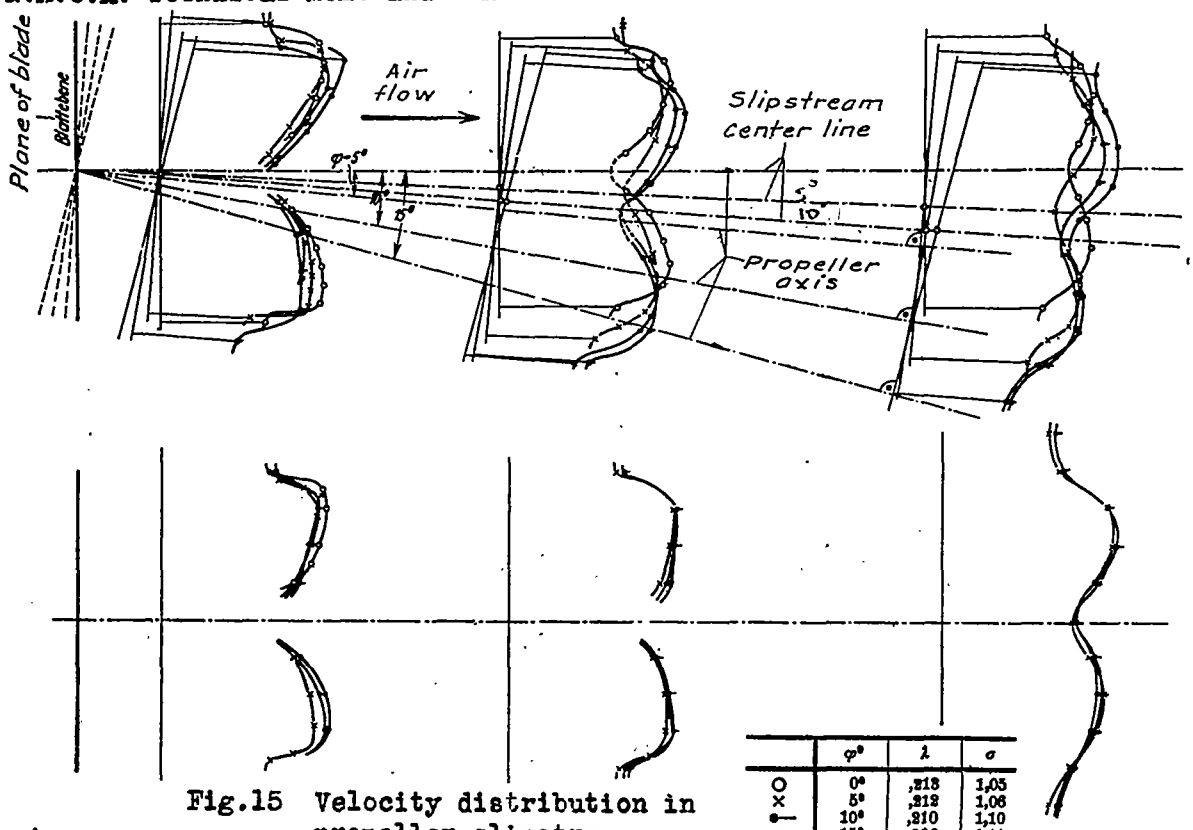

	φ°	λ	σ
○	0°	,218	1,05
×	5°	,212	1,06
●—	10°	,210	1,10
●	15°	,206	1,11

Fig.15 Velocity distribution in propeller slipstream.

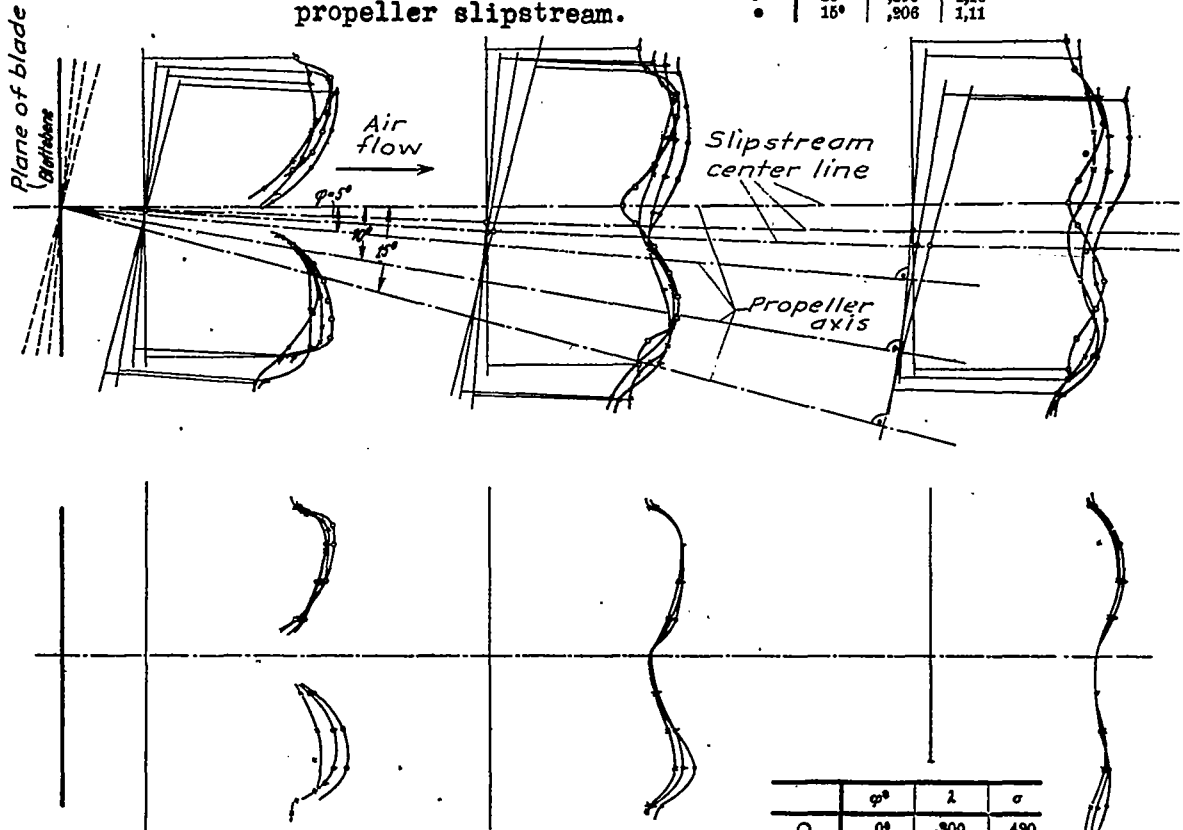

	φ°	λ	σ
○	0°	,300	,420
×	5°	,299	,420
●—	10°	,295	,425
●	15°	,290	,434

Fig.16 Velocity distribution in propeller slipstream.